

Semiconductor-topological insulator transition of two-dimensional SbAs induced by biaxial tensile strain

Shengli Zhang,¹ Meiqiu Xie,¹ Bo Cai,¹ Haijun Zhang,² Yandong Ma,³ Zhongfang Chen,² Zhen Zhu,⁴ Ziyu Hu,^{5,*} and Haibo Zeng^{1,†}

¹*Institute of Optoelectronics & Nanomaterials, Jiangsu Key Laboratory of Advanced Micro & Nano Materials and Technology, College of Material Science and Engineering, Nanjing University of Science and Technology, Nanjing 210094, China*

²*Department of Chemistry, Institute for Functional Nanomaterials, University of Puerto Rico, Rio Piedras, San Juan, Puerto Rico 00931, USA*

³*Department of Physics and Science, Jacobs University Bremen, Campus Ring 1, 28759 Bremen, Germany*

⁴*Materials Department, University of California, Santa Barbara, California 93106, USA*

⁵*Beijing Computational Science Research Center, Beijing 100094, China*

(Received 22 February 2016; revised manuscript received 2 May 2016; published 9 June 2016)

A stibarsen [derived from Latin *stibium* (antimony) and arsenic] or allemontite, is a natural form of arsenic antimonide (SbAs) with the same layered structure as arsenic and antimony. Thus, exploring the two-dimensional SbAs nanosheets is of great importance to gain insights into the properties of group V-V compounds at the atomic scale. Here, we propose a class of two-dimensional V-V honeycomb binary compounds, SbAs monolayers, which can be tuned from semiconductor to topological insulator. By *ab initio* density functional theory, both α -SbAs and γ -SbAs display a significant direct band gap, while others are indirect semiconductors. Interestingly, in an atomically thin β -SbAs polymorph, spin-orbital coupling is significant, which reduces its band gap by 200 meV. Especially under biaxial tensile strain, the gap of β -SbAs can be closed and reopened with concomitant change of band shapes, which is reminiscent of band inversion known in many topological insulators. In addition, we find that the Z_2 topological invariant is 1 for β -SbAs under the tensile strain of 12%, and the nontrivial topological feature of β -SbAs is also confirmed by the gapless edge states which cross linearly at the Γ point. These ultrathin group-V-V semiconductors with outstanding properties are highly favorable for applications in alternative optoelectronic and quantum spin Hall devices.

DOI: [10.1103/PhysRevB.93.245303](https://doi.org/10.1103/PhysRevB.93.245303)

I. INTRODUCTION

In recent years, two-dimensional (2D) nanosheets composed from the group-IVA elements, including graphene, silicene, germanene and stanene, have attracted significant interest due to their unique electronic, optical, and mechanical properties that differ from their bulk counterparts due to the reduced dimensionality [1–6]. However, graphene, silicene, germanene, and stanene are unlikely to replace silicon electronics because of their vanishing fundamental band gap. Even though with surface functionalization and external electric or strain fields, band gaps can be achieved [7–9], they are still too small for device applications.

Quite recently, a family of 2D crystals from the group-VA layered materials (P, As, Sb, Bi), has had a strong momentum of development [10–19]. Different from gapless graphene, silicene, germanene, and stanene of column IVA, the 2D nanosheets of the group-VA elements exhibit a significant fundamental band gap. For instance, a phosphorene monolayer can be exfoliated from bulk black phosphorus, and present a fundamental band gap of 2.0 eV, which is significantly larger than its bulk counterpart (0.3 eV) [19–23]. Quite recently, 2D monoelemental semiconductors, namely arsenene and antimonene (consisting of single-layer As and Sb atoms, respectively), with wide band gaps and high stability were predicted based on first-principles calculations [18]. Interestingly, although As and Sb are typically semimetals in the bulk, their

monolayers are indirect semiconductors with band gaps of 2.49 and 2.28 eV. The unique physical properties and promising electronics applications of these 2D monoelemental semiconductors (phosphorene, arsenene, and antimonene) have inspired significant amount of research interest on different aspects of these systems, such as highly anisotropic transport, negative Poisson's ratio, excellent optical and thermoelectric response, and perpendicular electric field or strain-induced 2D topological character [10–31].

Intriguingly, there exists a stibarsen [derived from Latin *stibium* (antimony) and arsenic] or allemontite, which is a natural form of arsenic antimonide (SbAs) [32]. The SbAs crystal has the same layered structure as arsenic and antimony with space group $R\bar{3}m$ No. 166. Specific exploration of the layered SbAs, which has not been synthesized so far, can provide precious insight to yet unexplored 2D V-V semiconductors at the atomic scale. A systematic theoretical investigation on their microstructures and properties can not only enhance our understanding of their intrinsic characteristics but also facilitate the applications of the family of V-V semiconductors.

Here we have established a basic physical picture of a family of group-V-V 2D semiconductors, namely, the unexplored SbAs with honeycomb structures, which can be tuned from semiconductor to topological insulator. By means of density functional theory (DFT) computations, we calculated the binding energies and phonon-band dispersions of SbAs polymorphs, which confirmed their thermodynamic and kinetic stabilities. We found that both α -SbAs and γ -SbAs are direct band-gap semiconductors, while others are indirect semiconductors. Among the honeycomb α -, β -, γ -, δ -, and ε -SbAs nanosheets, β -SbAs with a buckled structure is the

*huziyu@csrc.ac.cn

†zeng.haibo@njust.edu.cn

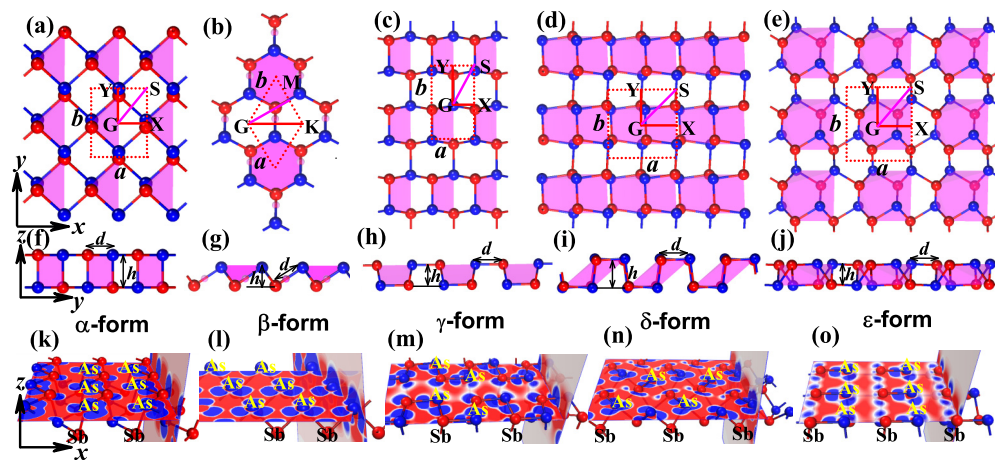


FIG. 1. Optimized structural configurations of monolayer arsenic antimonide (SbAs) polymorphs, which are displayed in both top views and side views from two horizontal directions: top views of (a) α -SbAs, (b) β -SbAs, (c) γ -SbAs, (d) δ -SbAs, and (e) ϵ -SbAs; side views of (f) α -SbAs, (g) β -SbAs, (h) γ -SbAs, (i) δ -SbAs, and (j) ϵ -SbAs. (k–o) are their corresponding charge density difference, respectively. Only β -SbAs shows hexagonal structure, while other SbAs polymorphs have orthorhombic crystal structures.

most stable configuration, and its bulk counterpart exists under standard conditions. Interestingly, a robust spin-orbital coupling in atomically thin β -SbAs polymorph results in a band-gap reduction of 200 meV. Under biaxial tensile strain, the gap of β -SbAs can be closed and reopened with a concomitant change of band shapes, which is reminiscent of band inversion known in many topological insulators. We further confirmed the nontrivial topological feature of the β -SbAs monolayer by the gapless edge states that cross linearly at the Γ point under the tensile strain of 12%. Therefore, the 2D β -SbAs monolayer is a promising candidate to realize the quantum spin Hall (QSH) effect.

II. COMPUTATIONAL DETAILS

The calculations were performed using the Vienna *ab initio* simulation package (VASP) [33]. The exchange-correlation term is described within the generalized gradient approximation (GGA) parametrized by the Perdew-Burke-Ernzerhof (PBE) functional [34]. A vacuum region greater than 20 Å perpendicular to the sheets (along the c axis) is applied to avoid the interaction between layers caused by the periodic boundary condition (PBC). For the geometry optimization, a kinetic-energy cutoff for plane-wave expansion is set to 500 eV. All the atoms in the unit cell are fully relaxed until the force on each atom is less than 0.005 eV/Å. Electronic minimization was performed with a tolerance of 10^{-5} eV. The Brillouin-zone sampling was carried out with a $21 \times 21 \times 1$ Monkhorst-Pack [35] grid for 2D sheets. The PBE calculations used scalar-relativistic PAW potentials, where both the core and the valence orbitals are treated using a scalar-relativistic Hamiltonian. Spin-orbital coupling (SOC) effects were included self-consistently up to second order (LS coupling) [36]. Since the SOC term is large just close to the core, the corresponding contributions to the Hamiltonian are only evaluated inside the PAW spheres using all-electron partial waves. Phonon dispersion relations with the finite displacement method, Raman spectra, and scanning

microscope images were calculated at the PBE level of theory using the CASTEP code [37,38].

III. RESULTS AND DISCUSSION

A. Structures and stabilities of SbAs monolayers

We investigated five typical honeycomb polymorph structures (α , β , γ , δ , ϵ , Fig. 1) in order to reveal intriguing possibilities to tune the electronic properties of SbAs by changing the honeycomb crystal structures. These five 2D models are potentially stable because they either correspond to an individual layer of bulk SbAs (buckled β phase) or are predicted as stable allotropes of other 2D group-VA nanosheets [39–41].

The α -SbAs has a hingelike layered structure [Fig. 1(a)] similar to phosphorene, which can be viewed as a deformed honeycomb structure of graphene. This hinge distorted atomic structure is distinctly different along the zigzag (x) and armchair (y) directions, which leads to anisotropic properties of α -SbAs. The α -SbAs monolayer contains four atoms per unit cell, and each atomic species is covalently bonded to three neighbors of the other atomic species. Thus, in each atom lone-pair electrons push its three bonds towards a tetrahedral coordination, forming a sp^3 covalent network with a waved structure.

The ground-state configuration of the β -SbAs monolayer mimics the metallic SbAs (111) surface [Fig. 1(b)], and the buckled β -SbAs honeycomb monolayer is also similar to those of buckled silicene, germanene, and stanene. In fact, the counterpart bulk material of the β -SbAs monolayer is the rhombohedral structure with the space group ($R\bar{3}m$) under standard conditions. As shown in Fig. 1(b), the β -SbAs monolayer is isotropic, which differs significantly from the anisotropic structure of α -SbAs. The buckled zigzag structure in the cross section of β -SbAs also differs from the distinct armchair ridges that result in the anisotropy of α -SbAs [Figs. 1(f) and 1(g)].

Other 2D structures, e.g., γ -, δ -, and ϵ -SbAs have rectangular unit cells, which contain four, eight, and eight atoms

TABLE I. Optimized structure parameters of SbAs polymorphs: a and b (Å) are lattice constants; h (Å) is the height of the SbAs monolayers. g is the band gap value of SbAs polymorphs calculated by PBE and PBE+SOC. The Δ_1 and Δ_2 (eV) are the gap differences of SbAs polymorphs between g^{PBE} and $g^{\text{SOC+PBE}}$.

Models	a	b	h	g^{PBE}	$g^{\text{SOC+PBE}}$	Δ_1	Δ_2
α -SbAs	4.04	4.75	2.62	0.22	0.19	0.03	0.04
β -SbAs	3.86	3.86	1.52	1.47	1.27	0.20	0.23
γ -SbAs	3.85	6.23	1.84	0.82	0.74	0.08	0.08
δ -SbAs	6.14	6.22	2.63	0.53	0.49	0.04	0.03
ε -SbAs	6.77	7.22	1.87	1.28	1.15	0.13	0.12

per unit cell [Figs. 1(c)–1(e)], respectively. Detailed structure parameters of these five SbAs polymorphs are shown in Table I.

Since As has a similar electronegativity with Sb, As-Sb bonds in 2D SbAs nanosheets are nonpolar and covalent. The covalent bonding nature between As and Sb is further supported by the calculated charge density difference [Figs. 1(k)–1(o)], where electron transfer between As and Sb is not observed. In addition, α - and β -SbAs have similar vibration spectra (see the following), indicating a very similar bonding nature.

In order to evaluate the thermodynamic stability of 2D SbAs nanosheets, we calculated the cohesive energy calculations for all SbAs polymorphs. The cohesive energy of SbAs is defined as the energy gained in assembling the SbAs nanosheets from its isolated constituent atoms by the equation $E_{\text{coh}} = (E_{\text{Sb}_n\text{As}_n} - nE_{\text{Sb}} - nE_{\text{As}})/n$. Here, $E_{\text{Sb}_n\text{As}_n}$, E_{Sb} , and E_{As} are the total energies of the SbAs monolayer, a single Sb atom, and a single As atom, respectively. Figure 2 summarizes the relative cohesive energies of SbAs monolayers with respect

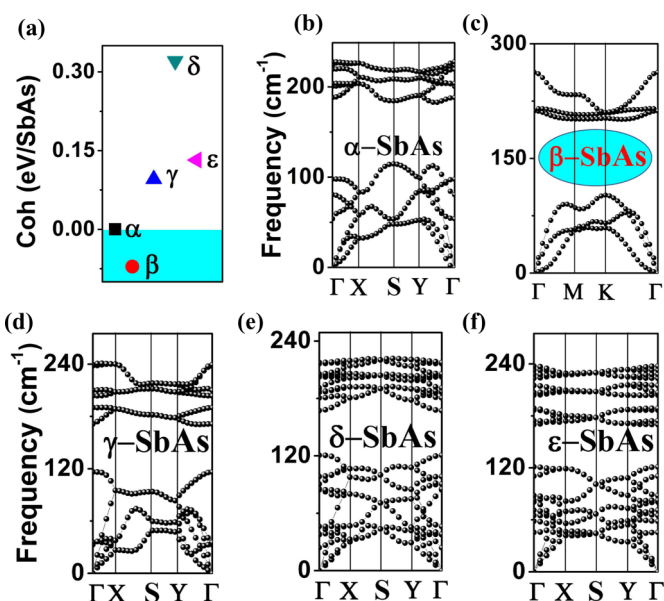


FIG. 2. (a) Calculated cohesive energy of SbAs monolayers. α -SbAs is taken as reference. Phonon-band dispersions of all monolayered arsenic antimonide (SbAs) polymorphs: (b) α -SbAs, (c) β -SbAs, (d) γ -SbAs, (e) δ -SbAs, and (f) ε -SbAs. No soft mode present in these structures.

to that of α -SbAs. Among the honeycomb α -, β -, γ -, δ -, and ε -SbAs nanosheets, β -SbAs with a buckled structure is the lowest-energy configuration. In fact, the bulk counterpart of the β -SbAs monolayer exists under standard conditions.

To gain insight into the structural stability of these SbAs monolayers, we have examined their phonon spectra [42]. As shown in Fig. 2, no soft phonon modes are observed for all 2D SbAs, indicating that these freestanding SbAs monolayers are indeed stable.

Considering the successful fabrication of graphene, MoS₂, phosphorene by exfoliation, and epitaxial growth on specific substrates, we believe that novel 2D SbAs nanosheets can be synthesized in the laboratory in the near future.

B. Electronic properties of SbAs monolayers

Since structure variety can lead to unprecedented richness in their fundamental electronic properties, it is intriguing to investigate the electronic structures of these SbAs monolayers. We have computed the band structures of 2D SbAs polymorphs (Fig. 3). Considering that significant spin-orbital coupling in the heavy element Sb is likely to alter the electronic band structure, we have included the SOC effect explicitly in our calculations. Figure 3 shows the band structure of monolayered SbAs polymorphs, which were calculated by the PBE method with and without SOC.

Comparing the band structures of SbAs monolayers with and without SOC, we find that the band structures share similar features. Namely, regardless of whether SOC is considered or not, both α -SbAs and γ -SbAs are direct semiconductors, while others are indirect semiconductors. For α -SbAs, the valence band maximum (VBM) and the conduction band minimum (CBM) both are located at X' , resulting in a direct band gap of 0.22 eV for PBE without SOC and 0.19 eV for PBE with SOC. Similarly, for γ -SbAs both VBM and CBM are located at the Γ high point, yielding a direct band gap of 0.82 eV for PBE without SOC (0.74 eV with SOC). In addition, for α -SbAs and γ -SbAs, both the top of the valence band and the bottom of the conduction are very dispersive, indicating light hole and electron effective mass. Thus, the combination of suitable direct band gaps and light carrier mass would turn SbAs into an excellent contender for a generation of ultrathin, flexible 2D electronic and optoelectronic devices.

To gain a deeper insight into the electronic properties, we computed the partial density of states (PDOS) of SbAs monolayers, as shown in Fig. 4, and in Fig. S1 in the Supplemental Material [43]. The PDOS analysis reveals that the states at the band edges, as well as at the lower-lying conduction band and the higher-lying valence band, originate from the hybridization of As 3*p* and Sb 4*p* orbitals (Fig. 4). For β -SbAs, without SOC, its VBM is mainly contributed by the As p_z and Sb p_z states, while when the SOC effect is considered, Sb p_z contributions are increased for VBM, which also includes partial Sb p_x and p_y states. The CBM of β -SbAs without SOC is mainly contributed by the As p_z state, while the CBM with SOC mainly comes from As p_z and Sb p_z states. Meanwhile, we computed the partial charge densities corresponding to the VBM and CBM of all SbAs monolayers (Figs. S1 and S2 [43]). For example, for β -SbAs, the CBM is mainly localized at the As sites without SOC. However, when

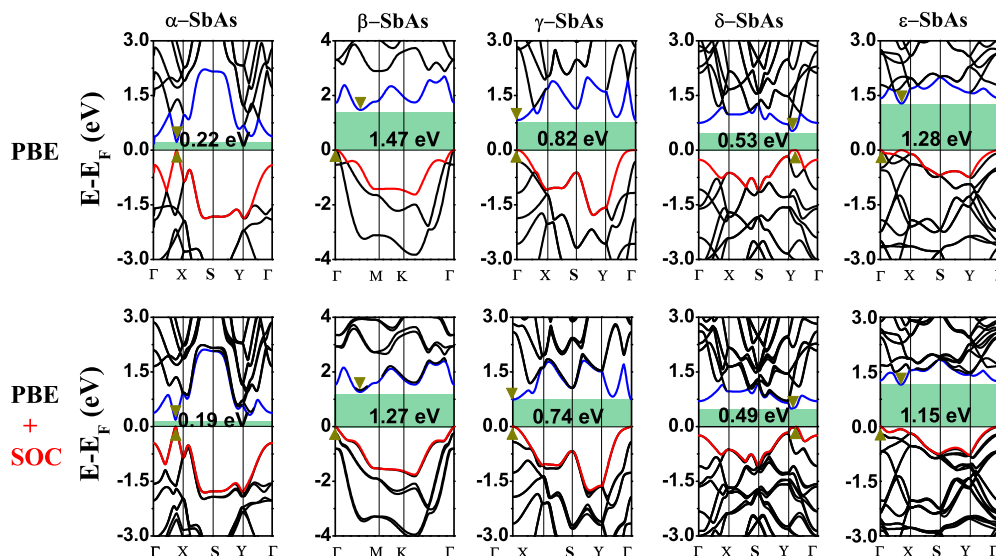


FIG. 3. Electronic band structures of monolayer SbAs polymorphs, which are calculated at the PBE level with SOC (lower panel) and without SOC (upper panel). The horizontal lines indicate the top of the valence band. The VBM and CBM are highlighted by blue and red lines.

the SOC effect is included, the CBM is localized at both As and Sb sites, consistent with the PDOS results.

To ensure the accuracy of the calculated variation trends for the energy band gaps, we further computed the band structures at the HSE06 level including the SOC effect (Fig. S3 [43]). Regardless whether SOC is considered or not, the band structures by HSE06 (Fig. S3) have the same variation trend as those obtained by GGA/PBE (Fig. S3 [43]). For example, α -SbAs and γ -SbAs are still direct band-gap semiconductors, and others show indirect band-gap semiconductor characteristics. In short, our HSE06-calculated band structures indicate that the freestanding SbAs monolayers' own versatile energy band gaps range from 0.70 to 2.13 eV (from 0.66 to 1.90 eV

with SOC), which is helpful for broadband photoresponse in practical optoelectronic applications.

As shown in previous paragraphs, the effect of SOC is significant in SbAs, which can reduce the band gap values and even modify the characters of frontier states. As a result, it is essential to consider SOC to elucidate the intrinsic properties of these 2D polymorphs. In fact, a strong SOC effect has also been found in antimonene [29] and arsenene [30], in which band inversion takes place in the vicinity of the Γ point when a biaxial tensile strain larger than 14.5% is applied, leading to six tilted Dirac cones in the Brillouin zone. SOC effect opens up a topologically nontrivial band gap at the Dirac points, exhibiting the features of 2D topological insulators [29]. Analogous to previous studies, SbAs structures are also expected to exhibit unique topological properties.

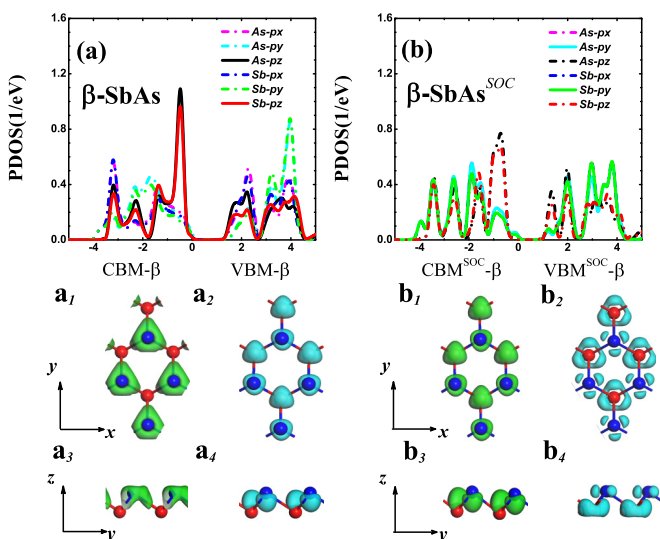


FIG. 4. The partial density of states (PDOS) and the isosurfaces of charge density distribution of VBM and CBM for SbAs monolayers calculated at the PBE level with and without SOC. The tops of the valence bands are set at zero.

C. Quantum spin Hall insulators in strain-modified β -SbAs

Taking into account the robust SOC effect in β -SbAs, can we achieve the nontrivial topological phase in this 2D β -SbAs material? For the semiconducting nanosheet, strain engineering is a favorable strategy to induce a switch between a trivial and a nontrivial topological phase in the system. Is it possible to use external tensile strain to induce a transition from a trivial phase to a topologically nontrivial phase for the β -SbAs monolayer?

To address this question, we firstly calculated the band structures of the monolayered β -SbAs under biaxial tensile strains (Fig. 5) at the PBE level (the results also have been given in Fig. S4 [43]). The structure changes of the β -SbAs monolayer under in-layer biaxial tensile strain can be seen in Fig. S5 [43]. Meanwhile, to check the possibility of the realization of this material under external strain, we performed the phonon spectra calculations. As shown in Fig. S6 [43], the systems are even stable when the strain reaches 18%. Under 0%–1% tensile strain, the CBM of monolayered β -SbAs remains in the Brillouin zone halfway between the Γ and M

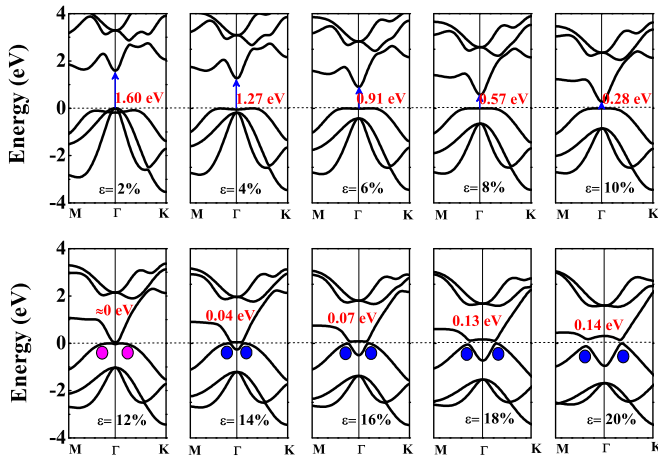


FIG. 5. Electronic band structures of monolayer β -SbAs under biaxial tensile strain at PBE level of theory with SOC. The horizontal dashed lines indicate the Fermi level. The band gap of β -SbAs is closed at $\varepsilon = 12\%$, and then is reopened associated with an intriguing change of band shape, which is reminiscent of band inversion and characterizes many known TIs.

high-symmetry points. However, further increasing the strain up to 2% shifts the CBM to the Γ high-symmetry points, which rapidly transforms monolayered β -SbAs into a direct band-gap semiconductor. The direct band gap persists under a tensile strain of 2%–10%. With a 10% strain, there is still a direct band gap of 0.28 eV. Such a trend eventually leads to gap closing at the Γ high-symmetry point when the strain is 12% (14.8% at the HSE06 level). Excitingly, the band gap opens again when the strain is larger than 12%. However, the maximum valence band is transformed from the “ Λ shape” to the “ M shape,” and the minimum conduction band is flattened near the Γ high-symmetry point. As a result, the β -SbAs monolayer becomes an indirect band-gap semiconductor again. The gap closing and reopening associated with the change of band shapes is reminiscent of band inversion, which characterizes many known topological insulators (TIs) [44–46]. In order to ascertain the topological phase transition in the strained β -SbAs monolayer, we calculate the Z_2 topological invariants. $Z_2 = 1$ suggests a topologically nontrivial state, while $Z_2 = 0$ corresponds to a trivial state. Since inversion symmetry is absent in this system, the Z_2 invariants cannot be determined from the parities of the filled states. To this end, we have used the n -field configuration method [47]. We find that the Z_2 topological invariant is 0 for β -SbAs with the tensile strain of 10%, while it is $Z_2 = 1$ for β -SbAs with the tensile strain of 12%. These results firmly demonstrate that there is indeed a strain-induced topological phase transition in β -SbAs. Therefore, compared to the case of antimonene, the β -SbAs monolayer is also expected as a potential candidate to achieve the QSH effect.

The 2D nontrivial insulating state is often characterized by topologically protected conducting edge states within the bulk gap [48–50]. Thus, the β -SbAs monolayer under the tensile strain of 12% should hold an odd number of topologically protected Dirac-like edge states connecting the conduction- and valence-band edges at Γ high-symmetry points.

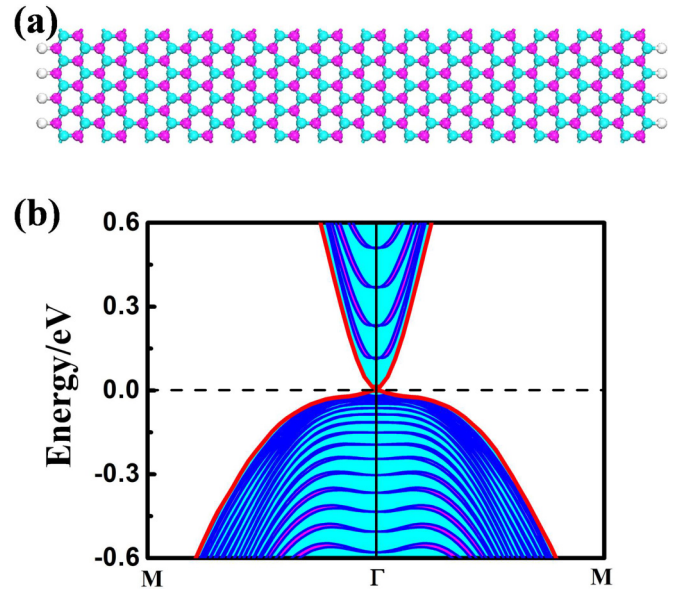


FIG. 6. (a) Top view of β -SbAs nanoribbon (over 10 nm) with zigzag edges under tensile strain. The unsaturated atoms in the zigzag nanoribbon edges are terminated by hydrogen atoms to eliminate all dangling bonds. (b) Electronic band structures of the β -SbAs nanoribbon at $\varepsilon = 12\%$. The helical edge states (red lines) can be clearly identified around the Γ point. The horizontal dashed lines indicate the Fermi level.

To further confirm the nontrivial features of the β -SbAs monolayer under the tensile strain of 12%, we construct a zigzag β -SbAs nanoribbon structure, and the edge unsaturated atoms are terminated by hydrogen atoms to eliminate all dangling bonds. The width of the zigzag β -SbAs nanoribbon adopted here is 10 nm, which is enough to avoid interactions between edge states of the two sides. The band structure of the zigzag β -SbAs nanoribbon is shown in Fig. 6. The gapless edge states appear and cross linearly at the Γ point, which further confirms the nontrivial topological phase in the β -SbAs monolayer under the tensile strain of 12%. Thus, our results provide a promising strategy for designing 2D V-V QSH insulators.

D. Characterization analysis of SbAs

We further calculated the Raman spectra and scanning tunneling microscope (STM) images (Fig. 7) in order to gain insights into the electronic structure and surface morphology, and to assist future experimental characterization. For α -SbAs, which belongs to the C_{2v} group, its Raman active modes are A_1 at 52 cm^{-1} , B_2 at 194 cm^{-1} , B_1 at 51 cm^{-1} , which exhibit prominent Raman scattering. Both A_1 and B_1 modes are out-of-plane vibrating mode, while the B_2 mode is an in-plane vibrating mode. For β -SbAs with the C_{3v} group, the Raman active modes are at E at 216 cm^{-1} . The in-plane E modes are doubly degenerated with two atoms in the SbAs unit cell vibrating along opposite directions. For γ -, δ -, and ε -SbAs, with four, eight, and eight atoms per unit cell, respectively, their Raman active modes are also clearly shown in Fig. 7. To help recognize the polymorphs in future experiments, STM images of all SbAs polymorphs are simulated at $+2.0 \text{ V}$ bias

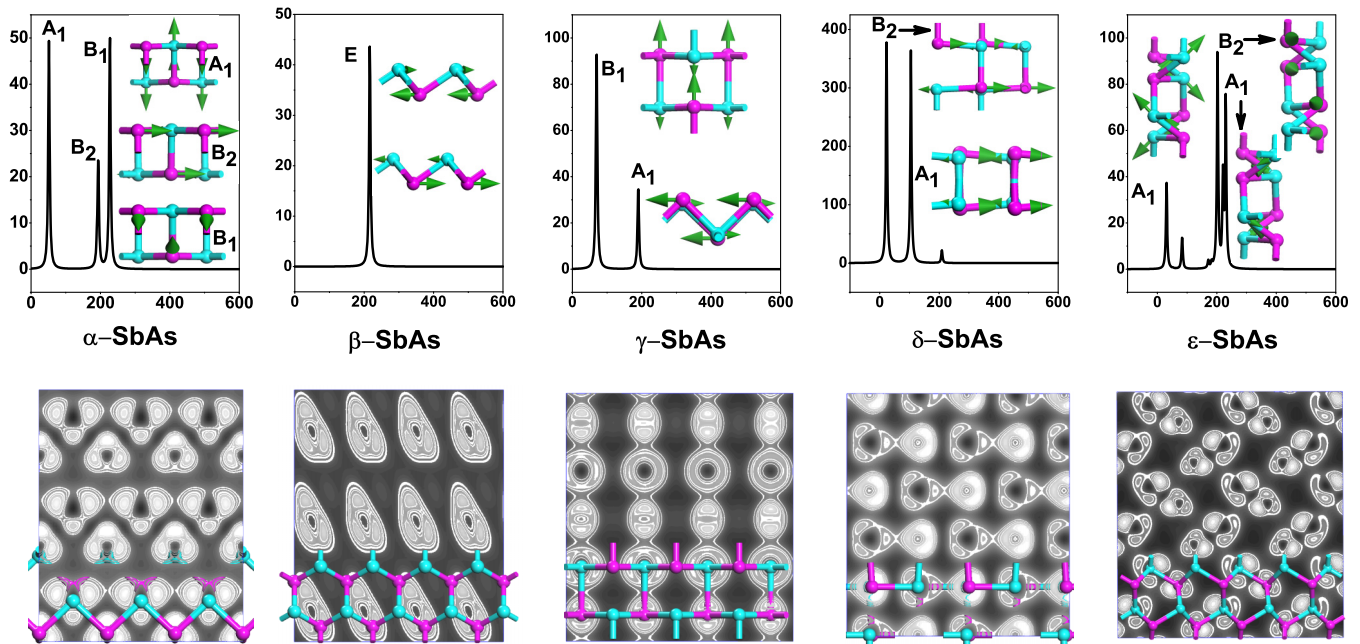


FIG. 7. Calculated Raman spectra of monolayer SbAs polymorphs, with the corresponding vibrational modes. Meanwhile, we also provide our simulated scanning microscope (STM) images at +2.0 V bias of SbAs polymorphs.

(Fig. 7). We expect that these features of 2D SbAs provide more information for identifying these monolayered polymorphs, and also improve the possibility of their synthesis in the near future.

IV. SUMMARY

We establish a basic physical picture of a family of group-VA-VA 2D semiconductors, namely, the unexplored SbAs with distinguished honeycomb polymorph structures based on DFT computations. Our calculated binding energies and phonon-band dispersions of SbAs polymorphs suggest their outstanding thermodynamic and kinetic stabilities. Among the honeycomb α , β , γ , δ , and ε -SbAs nanosheets, β -SbAs with a buckled structure is the lowest-energy configuration, and its corresponding counterpart bulk material exists under standard conditions. Regardless of whether SOC is considered or not, both α -SbAs and γ -SbAs are direct semiconductors, while others are indirect semiconductors. Different from other polygraphs, the β -SbAs has a 200-meV band-gap reduction when SOC is included, highlighting the significance of the SOC effect. Interestingly, we find that the gap closing and

reopening of β -SbAs is associated with TI characteristics. Therefore, akin to the case of antimonene and arsenene, the β -SbAs monolayer is also expected as a potential candidate to achieve the QSH effect. We believe that these unexplored 2D group VA-VA semiconductors, as exemplified by SbAs monolayers, will lead to a large family of 2D semiconductors with intriguing electronic properties.

ACKNOWLEDGMENTS

This work was supported by National Key Basic Research Program of China (Grant No. 2014CB931702), NSFC (Grants No. 51572128 and No. 21403109), NSFC-RGC (Grant No. 5151101197), NSF of Jiangsu province (No. BK20140769), the Fundamental Research Funds for the Central Universities (Grant No. 30916015106), and in the USA by DoD (Grant No. W911NF-15-1-0650) and NSF (Grant No. EPS-1002410), Scientific computing and simulation of physical systems (Grant No. U1530401). We also acknowledge Computer Network Information Center (supercomputing center) of Chinese Academy of Sciences (CAS) for allocation of computing resources.

- [1] K. S. Novoselov, A. K. Geim, S. V. Morozov, D. Jiang, Y. Zhang, S. A. Dubonos, and A. Firsov, *Science* **306**, 666 (2004).
- [2] K. S. Novoselov, D. Jiang, F. Schedin, T. J. Booth, V. V. Khotkevich, S. V. Morozov, and A. K. Geim, *Proc. Natl. Acad. Sci. U. S. A.* **102**, 10451 (2005).
- [3] C. C. Liu, W. Feng, and Y. Yao, *Phys. Rev. Lett.* **107**, 076802 (2011).
- [4] L. Tao, E. Cinquanta, D. Chiappe, C. Grazianetti, M. Fanciulli, M. Dubey, and D. Akinwande, *Nat. Nanotechnol.* **10**, 227 (2011).
- [5] Z. Ni, Q. Liu, K. Tang, J. Zheng, J. Zhou, R. Qin, and J. Lu, *Nano Lett.* **12**, 113 (2011).
- [6] F. F. Zhu, W. J. Chen, Y. Xu, C. L. Gao, D. D. Guan, C. H. Liu, and J. F. Jia, *Nat. Mater.* **14**, 1020 (2015).
- [7] Y. Pan, L. Zhang, L. Huang, L. Li, L. Meng, M. Gao, and H. J. Gao, *Small* **10**, 2215 (2014).
- [8] Y. Zhang, T. T. Tang, C. Girit, Z. Hao, M. C. Martin, A. Zettl, and F. Wang, *Nature* **459**, 820 (2009).
- [9] X. Li, X. Wang, L. Zhang, S. Lee, and H. Dai, *Science* **319**, 1229 (2008).

- [10] L. Li, Y. Yu, G. J. Ye, Q. Ge, X. Ou, H. Wu, and Y. Zhang, *Nat. Nanotechnol.* **9**, 372 (2014).
- [11] C. Kamal and M. Ezawa, *Phys. Rev. B* **91**, 085423 (2015).
- [12] Z. Zhu, J. Guan, and D. Tománek, *Phys. Rev. B* **91**, 161404 (2015).
- [13] O. Ü. Aktürk, V. O. Özçelik, and S. Ciraci, *Phys. Rev. B* **91**, 235446 (2015).
- [14] Z. Zhu and D. Tománek, *Phys. Rev. Lett.* **112**, 176802 (2014).
- [15] M. Wu, H. Fu, L. Zhou, K. Yao, and X. C. Zeng, *Nano Lett.* **15**, 3557 (2015).
- [16] G. Wang, W. J. Slough, R. Pandey, and S. P. Karna, *ACS Appl. Mater. Interfaces* **1508**, 07461 (2015).
- [17] H. Liu, A. T. Neal, Z. Zhu, Z. Luo, X. Xu, D. Tománek, and P. D. Ye, *ACS Nano* **8**, 4033 (2014).
- [18] S. Zhang, Z. Yan, Y. Li, Z. Chen, and H. Zeng, *Angew. Chem., Int. Ed.* **127**, 3155 (2015).
- [19] S. Zhang, M. Xie, F. Li, Z. Yan, Y. Li, E. Kan, W. Liu, Z. Chen, and H. Zeng, *Angew. Chem., Int. Ed.* **55**, 1666 (2016).
- [20] L. Kou, T. Frauenheim, and C. Chen, *J. Phys. Chem. Lett.* **5**, 2675 (2014).
- [21] R. Fei and L. Yang, *Nano Lett.* **14**, 2884 (2014).
- [22] J. W. Jiang and H. S. Park, *Nat. Commun.* **5**, 4727 (2014).
- [23] Q. Liu, X. Zhang, L. B. Abdalla, A. Fazzio, and A. Zunger, *Nano Lett.* **15**, 1222 (2015).
- [24] X. Yu, S. Zhang, H. Zeng, Q. Wang, *Nano Energy* **25**, 34 (2016).
- [25] S. Zhang, Y. Hu, Z. Hu, B. Cai, and H. Zeng, *Appl. Phys. Lett.* **107**, 022102 (2015).
- [26] Y. D. Ma, Y. Dai, L. Kou, T. Frauenheim, and T. Heine, *Nano Lett.* **15**, 1083 (2015).
- [27] P. F. Zhang, Z. Liu, W. Duan, F. Liu, and J. Wu, *Phys. Rev. B* **85**, 201410 (2012).
- [28] Z. Liu, C. X. Liu, Y. S. Wu, W. H. Duan, F. Liu, and J. Wu, *Phys. Rev. Lett.* **107**, 136805 (2011).
- [29] Z. Song, C. C. Liu, J. Yang, J. Han, M. Ye, B. Fu, Y. Yang, Q. Niu, J. Lu, and Y. Yao, *NPG Asia Mater.* **6**, e147 (2014).
- [30] M. W. Zhao, X. M. Zhang, and L. Y. Li, *Sci Rep.* **5**, 16108 (2015).
- [31] H. Zhao, Y. Ma, and Z. Chen, *Nanoscale* **7**, 19152 (2015).
- [32] P. Quensel, K. Ahlborg, and A. Westgren, *Geologiska Foeren. Stockholm Foerh.* **59**, 135 (1937).
- [33] G. Kresse and J. Furthmüller, *Phys. Rev. B* **54**, 11169 (1996).
- [34] J. P. Perdew, K. Burke, and M. Ernzerhof, *Phys. Rev. Lett.* **77**, 3865 (1996).
- [35] H. J. Monkhorst and J. D. Pack, *Phys. Rev. B* **13**, 5188 (1976).
- [36] X. L. Qi and S. C. Zhang, *Rev. Mod. Phys.* **83**, 1057 (2011).
- [37] S. J. Clark, M. D. Segall, C. J. Pickard, P. J. Hasnip, M. I. Probert, K. Refson, and M. C. Payne, *Z. Kristallogr.* **220**, 567 (2005).
- [38] K. Refson, P. R. Tulip, and S. J. Clark, *Phys. Rev. B* **73**, 155114 (2006).
- [39] Z. Zhu, J. Guan, D. Liu, and D. Tománek, *ACS Nano* **9**, 8284 (2015).
- [40] J. Guan, Z. Zhu, and D. Tománek, *ACS Nano* **8**, 12763 (2014).
- [41] Z. Zhu, J. Guan, D. Liu, and D. Tománek, *Nano Lett.* **15**, 6042 (2015).
- [42] L. M. Yang, V. Bacic, I. A. Popov, A. I. Boldyrev, T. Heine, T. Frauenheim, and E. Ganz, *J. Am. Chem. Soc.* **137**, 2757 (2015).
- [43] See Supplemental Material at <http://link.aps.org/supplemental/10.1103/PhysRevB.93.245303> for more detailed structure, charge density distribution, density of states, band structures, and phonon dispersion for 2D SbAs.
- [44] H. Zhang, C. X. Liu, X. L. Qi, X. Dai, Z. Fang, and S. C. Zhang, *Nat. Phys.* **5**, 438 (2009).
- [45] Y. Xu, B. Yan, H. J. Zhang, J. Wang, G. Xu, P. Tang, W. Duan, and S. C. Zhang, *Phys. Rev. Lett.* **111**, 136804 (2013).
- [46] C. Si, J. Liu, Y. Xu, J. Wu, B. L. Gu, and W. Duan, *Phys. Rev. B* **89**, 115429 (2014).
- [47] T. Fukui and Y. Hatsugai, *J. Phys. Soc. Jpn.* **76**, 053702 (2007).
- [48] L. Y. Li, X. M. Zhang, X. Chen, and M. W. Zhao, *Nano Lett.* **15**, 1296 (2015).
- [49] Y. D. Ma, L. Z. Kou, A. J. Du, and T. Heine, *Nano Res.* **8**, 3412 (2015).
- [50] L. Z. Kou, Y. D. Ma, B. H. Yan, X. Tan, C. F. Chen, and S. C. Smith, *ACS Appl. Mater. Interfaces* **7**, 19226 (2015).